Journal of Materials Chemistry A

ROYAL SOCIETY OF CHEMISTRY

PAPER

View Article Online
View Journal | View Issue

Cite this: J. Mater. Chem. A, 2025, 13, 34696

Fluorine-free sulfonated polyhedral oligomeric silsesquioxanes: replacing polymeric binder in fuel cell catalyst layers

Julian Stiegeler, †[ab] Sophia K. Kilian, †[c] Marco Viviani,‡[c] Hannes Liepold,[acd] Carolin Klose,[ac] Andreas Münchinger*[ac] and Tym de Wild *[acd]

Received 14th April 2025
Accepted 27th August 2025

DOI: 10.1039/d5ta02947c

rsc.li/materials-a

One of the key points in transitioning to fluorine-free fuel cells is the development of fluorine-free ionomers for both membranes and electrodes. Promising materials, such as sulfonated phenylated polyphenylenes (sPPP) (*e.g.*, Pemion®) and sulfonated polyphenylene sulfones (sPPS), demonstrate low gas crossover, making them suitable for membrane applications. However, recent studies suggest that their low gas permeability combined with high swelling under humid conditions complicates their use in electrodes, particularly at high current densities. In this study, however, we explore cage-like sulfonated polyhedral oligomeric silsesquioxanes (sPOSS) as a proton-conductive material and electrode binder. We demonstrate the fabrication of stable electrodes using sPOSS, which exhibit performance comparable to hydrocarbon-based ionomers like sPPP in the kinetic region while outperforming it at high current densities, likely due to improved gas transport properties.

Introduction

Proton-exchange membrane fuel cells (PEM-FCs) are a viable alternative to combustion engines and battery-powered electric vehicles because of their high efficiency and short refueling times. The current state-of-the-art materials for these fuel cells are based on perfluorosulfonic acids (PFSAs), which serve as both the membrane material and the proton-conducting medium in the electrodes.

However, per- and polyfluoroalkyl substances are under critical review owing to their environmental persistence and bioaccumulation,[1–3] leading to discussions of a potential ban under the REACH regulation.[4] This has motivated efforts to develop alternative, more sustainable proton-conductive materials for fuel cell applications. Materials under investigation include sulfonated poly(phenylene sulfones) (sPPS),[5] which remain at laboratory scale, and commercially available materials such as Pemion® (sPPP).[6] While these materials perform well as membranes due to their low gas permeability, this property poses limitations when used as ionomers in electrodes, where good gas transport is essential.[7] Additionally, these materials experience excessive swelling when in contact with liquid water making it hard to formulate electrodes that can operate efficiently over a large relative humidity (RH) regime.[8]

This work introduces sulfonic acid-functionalized polyhedral oligomeric silsesquioxanes (sPOSS) as a potential alternative material for electrode binder and ionic conductor. sPOSS has previously been employed in membranes as a reinforcing or crosslinking agent, benefiting from high proton conductivity while increasing the dimensional stability of the membranes.[9,10] Additionally silica and sulfonated silica were used in membranes as additives to increase proton conductivity at low RH due to the hydrophilic nature of sulfonated silica.[11,12] Implementation of silica in the electrodes showed promising results in enhancing cell stability.[13–15] In this study, sPOSS is investigated as the sole binder and proton-conducting material in the cathode. It is shown to provide adequate proton conductivity while enhancing gas transport within the electrode, owing to increased porosity resulting from its particle-like structure. Although sPOSS contains eight phenyl groups per molecule, which could potentially lead to catalyst poisoning through phenyl adsorption, as reported for other hydrocarbon-based ionomers, we initially assumed that such interactions would be minimized due to steric hindrance from the bulky sPOSS structure. The binder properties are likely a result of van der Waals or ionic interactions between the different materials.

[a]Electrochemical Energy Systems, IMTEK - Department of Microsystems Engineering, University of Freiburg, Georges-Koehler-Allee 103, 79110 Freiburg, Germany. E-mail: andreas.muenchinger@imtek.uni-freiburg.de; tym.de.wild@imtek.uni-freiburg.de

[b]University of Freiburg, Institute and FIT – Freiburg Center for Interactive Materials and Bioinspired Technologies (FIT), Georges-Koehler-Allee 105, 79110 Freiburg, Germany

[c]Hahn-Schickard, Georges-Koehler-Allee 103, 79110 Freiburg, Germany

[d]Freiburg Materials Research Center (FMF), University of Freiburg, Stefan-Meier-Straße 21, Freiburg, 79104, Germany

† Equally contributing authors.

‡ Current affiliation: UFI Hydrogen S.p.A. Corso General Cantore 39, 38061, Serravalle, Ala (TN), Italy.

We also highlight that in particle-based sPOSS systems, ionomer swelling is expected to behave differently compared to conventional film-forming ionomers. Initially, water will fill the void spaces between particles, followed by swelling that increases the interparticle distance. This contrasts with classic ionomers, which form continuous swollen films with a continuous ionomer phase. sPOSS and other silsesquioxanes are already widely available in industry at relatively low costs because of their use in personal healthcare products. This industrial availability could facilitate their introduction into fuel cells as a commercial product, as the scalability of material production is already established. Furthermore, the wide range of possible functionalisation make silsesquioxanes an interesting platform for new material development.[16]

Experimental

The authors acknowledge that the sPOSS used in later stages, is not an ionomer. However, as it serves a similar function in the fuel cell cathode, the term "ionomer" and the ionomer-to-carbon ratio (I/C) are used for consistency and easier comparability between systems and publications.

Synthesis of sPOSS

For the synthesis of sulfonic acid functionalized octaphenyl-POSS (sPOSS), we followed a synthesis route similar to the one proposed by Hartmann-Thompson *et al.*[9] In a round-bottom flask, chlorosulfonic acid (HSO_3Cl, 16.62 mL) was cooled in an ice bath. Under stirring, octaphenyl polyhedral oligomeric silsesquioxane (oPOSS) (5.168 g) was slowly added to prevent overheating. Once all the octaphenyl-POSS had been added, the ice bath was removed, and the solution was stirred at room temperature overnight.

The residual HSO_3Cl was removed by distillation under vacuum, first at 60 °C and then at 90 °C. A clear solid with a brownish tint was obtained.

The solid product was carefully crushed in the flask and dispersed in water. A white compound formed, which slowly precipitated. The mixture was filtered, and the solid was washed with 2 M HCl (300 mL), followed by deionized (DI) water until the filtrate was pH-neutral. The resulting solid was dried in a vacuum oven at 60 °C for 3 days, yielding sulfonated POSS (sPOSS).

sPOSS characterization

Ion exchange capacity (IEC). IEC was determined by titration with 0.01 M NaOH using an automated titrator (Eco Titrator, Metrohm) using a pH electrode (Porotrode, Metrohm) (for details see S1).

ATR-IR. ATR-IR was measured on a Nicolet Summit X FTIR spectrometer (Thermo Scientific) using the Golden Gate ATR accessory. All spectra were background corrected by OMNIC Paradigm v2.7.

Protonic bulk conductivity. Protonic conductivity of the bulk material after functionalisation was measured using a HP 4192A LF impedance analyzer. The hydration number (λ) was determined by mass (for details see S2).

Hydrolytic stability. Stability of the sPOSS material in water atmosphere was measured using and STA 449 F3 Jupiter TGA (Netzsch) with an sSTEAM water vapor generator (aDROP Feuchtemeβtechnik GmbH). Longterm stability was measured at 110 °C in saturated water vapour, using water-feed rate of 2 g h^{-1} at ambient pressure for 6 days.

Catalyst coated membrane (CCM) preparation

Ink fabrication. For the electrodes, different ionomers were used. For the anodes, PP1-HNN8-00-X (HNN8) with an IEC of 3.1 m eq. g^{-1} was implemented using Tanaka TEC10E50E Pt on carbon. On the cathode, the previously prepared sPOSS were used, utilizing Tanaka TEC10V50E. Before ink preparation, ionomer stock solutions were prepared at 1 and 5 wt% for sPOSS and HNN8, respectively. The ionomers were dissolved or dispersed in a mixture of DI-Water and isopropanol (IPA) with a mass ratio of 1 : 1 under continuous stirring at 40 °C, 300 rpm for 16 hours.

The electrode inks were prepared by mixing the catalyst with a mixture of DI-water and IPA (ratio 1 : 1 by mass) and the stock ionomer solution to achieve a solid content of 0.88 wt%. To get stable and homogenous inks, the dispersions were sonicated with a sonication horn (Hielscher Ultrasonic Technology, model UI250v) at 100% amplitude and cycling of 0.9 s s^{-1} for 1 h in an ice bath. The composition of the prepared inks are shown in Table 1.

CCM fabrication. CCMs were prepared by spray coating the electrodes on a Pemion® PF1-HLF8-15-X membrane (Ionomr Innovations Inc.). An ultrasonic spray system (Sono-Cell®, Sonaer Inc.) was used. All CCMs had a fixed Pt loading of 0.1 mg_{Pt} cm^{-2} for the anode and 0.4 mg_{Pt} cm^{-2} for the cathode.

Cell assembly. CCMs were laminated using 25 μm polyethylene naphtalate (PEN) gaskets for mechanical stabilization. These gaskets have a 4 cm^2 cutout, which defines the active area. For GDL/MPL, commercial Freudenberg H14CX653 was used on the anode and cathode side. To set the compression, glass-fiber reinforced PTFE (Böhme Kunstofftechnik®) with a nominal thickness of 110 μm were used as spacers. This leads to a local GDL/MPL thickness of 135 μm on the active area. The MEAs were assembled in commercial cell fixtures (Scribner LLC) with in-house 4 cm^2 parallel graphite flow fields in a cross-flow setup. The cell was sealed by applying 10 Nm torque on the eight M6 rods of the fixture.

Fuel cell testing

Cells were tested with a commercial test stand (850e Fuel Cell Test System, Scribner, LLC). All cells underwent a similar testing protocol, which started with a break-in followed by oxygen reduction kinetics followed by ECSA and H_2 crossover measurements. Subsequently, protonic resistance and polarization curves were determined at 95 °C, 50% RH, and 80% RH. Before break-in, every cell was leak-tested and heated up to 80 °C. An overview of all operation parameter for the different measurements are given in Table S3.

Table 1 Ink composition of the tested cells: the Pemion® based ink is used for all anodes as well as the cathode of the Pemion® reference cell, the sPOSS based inks are used as cathodes only

	Pemion®	sPOSS		
Ingredient	Mass [g]	Ink-0.1 mass [g]	Ink-0.2 mass [g]	Ink-0.3 mass [g]
TEC 10E50E	0.1	—	—	—
TEC 10V50E	—	0.1	0.1	0.1
DI-water	5.75	5.75	5.75	5.75
IPA	5.75	5.75	5.75	5.75
HNN8 5 wt% IPA : H_2O (1 : 1 wt)	0.21	—	—	—
sPOSS 1 wt% IPA : H_2O (1 : 1 wt)	—	0.54	1.06	1.60

Break-in procedure. 20 voltage cycles between OCV, 0.2 V and 0.5 V holding every potential for 30 s, at 80 °C, ambient pressure, 96% relative humidity (RH) and H_2/O_2 flow of 0.25/0.50 norm liters per minute (nlpm).[6]

Mass activity. The oxygen reduction reaction (ORR) kinetics, specifically mass activity measurements were taken under H_2/O_2 conditions (0.25/1.0 nlpm) at 80 °C, 100% RH, and 150 kPa_{abs}. A current-controlled polarization curve from 0 to 100 mA cm^{-2}, 1.25 mA cm^{-2} per point and from 100 to 400 mA cm^{-2}, 12.5 mA cm^{-2} per point all with a three-minute hold time per point was recorded. Measured potentials were corrected using the high-frequency resistance (HFR), measured at a fixed frequency of 3.2 kHz, and currents were adjusted for hydrogen crossover and membrane shorting current both extracted by linear sweep measurements (LSV) with H_2/N_2 (0.20/0.05 nlpm) at 80 °C, 96% RH, and 150 kPa. After corrections, mass activity was determined as the Pt-loading normalized current density at a potential of 0.9 V, following the methodology of Neyerlin *et al.*[17]

ECSA and hydrogen (H_2) crossover measurements. Before the measurement, the cathode compartment of the cell was flushed with nitrogen for a minimum of one hour to remove all molecular and absorbed oxygen species. For ECSA evaluation, cyclic voltammograms (CVs) were recorded under H_2/N_2, 0.20/0 nlpm (anode/cathode), 80 °C, 96% RH, and atmospheric pressure. The voltage was swept from 0.08 to 0.80 V *vs.* the anode at a scan rate of 25 mV s^{-1}. To achieve reliable results, the CVs were repeated 8 times. The electrochemical surface area (ECSA) was calculated based on the hydrogen adsorption and desorption peak of the last five cycles using known literature values for the hydrogen under potential deposition (H_{upd}) charge of polycrystalline Pt (210 μC cm^{-2}).[18,19] H_2 crossover was determined by LSV with a scan rate of 1 mV s^{-1}. The measurement was done in H_2/N_2 with a flow of 0.20/0.05 nlpm (anode/cathode) at 80 °C and 96% RH.

Protonic resistance. Protonic resistance was determined by impedance spectroscopy. Measured at 150 kPa_{abs} and H_2/N_2, flow 0.50/0.50 nlpm (anode/cathode). RH was either 80% or 50% RH. The measurements were performed at 0.45 V DC offset with an amplitude of 22.5 mV from 100 kHz to 0.2 Hz (20 points per decade). The protonic resistance was estimated *via* a fit of the impedance response to a 1D transmission line model.

Polarization curves. Polarization curves were obtained by galvanostatic measurements from low to high current density (0–62.5 mA cm^{-2}, 3.125 mA cm^{-2} per point, 1 min per point; 62.5–500 mA cm^{-2}, 31.25 mA cm^{-2} per point, 3 min per point; 500 – end mA cm^{-2}, 62.5 mA cm^{-2} per point, 3 min per point; data recorded as the average voltage at the last ten seconds). Measurements were performed at 95 °C and 150 kPa_{abs} in H_2/Air with flow 0.25/1.00 nlpm (anode/cathode). Gas inlet RH was either 80% or 50%.

Limiting current. For oxygen-limiting current measurement 1 cm^2 cells were used. The cells underwent break-in followed by the limiting current measurements. For the determination of pressure-independent mass transport resistance, oxygen limiting current was measured at 80 °C, 96% RH at 0.5 vol% of oxygen in nitrogen at 150, 200, 250, and 300 kPa_{abs} of back-pressure resulting in an average cell pressure of 172, 217, 264 and 312 kPa_{abs}, respectively. Between every oxygen concentration change the cell was equilibrated for one hour.[20]

Voltage cycling. For long-term stability test an accelerated test protocol derived from the US department of Energy (DOE) is used.[21] After break-in and beginning of test (BOT) testing the cell is cycled between 0.6 V and 0.95 V using a trapezoidal voltage curve with 2.5 s hold-time on each potential and a 0.5 s ramp time. The cells were operated under H_2/N_2, with flow of 0.05/0.02 nlpm (anode/cathode) at 80 °C and 96% RH and ambient pressure.

SEM cross-sections and EDX. Cross sections of the catalyst layer were prepared and analyzed using a focused ion beam scanning electron microscope (FIB-SEM, Scios 2 HiVac, FEI Company). To facilitate imaging, the samples were cryogenically fractured in liquid nitrogen, mounted on aluminum SEM stubs (Science Services GmbH) with conductive carbon adhesive tabs, and sputtered with gold for 15 s. A protective platinum layer was deposited using a gas injection system (GIS) to shield the targeted areas before ion milling. Ga+ ions at 30 kV and 50 nA were used for material ablation, creating a cross-section approximately 50 μm in width, followed by a final polishing step at 7 nA.

High-resolution micrographs were acquired at an acceleration voltage of 10 kV, a working distance of approximately 7 mm, and a beam current of 50 pA, using an Everhart-Thornley (ET) detector. Catalyst layer thickness was determined by measuring 20 points and correcting for the 52° stage tilt.

For energy-dispersive X-ray spectroscopy (EDX), a scanning electron microscope (SEM, Maia 3, Tescan GmbH) equipped with an EDX detector (Oxford Instruments) was used. EDX maps were acquired at an acceleration voltage of 20 kV with a working distance of 7 mm.

Transmission electron microscopy (TEM). For TEM analysis, the sample was prepared by spraycoating one layer of sPOSS-0.3 onto a TEM grid (CF200F2-Cu-UL, Electron Microscopy Sciences) during CCM fabrication. TEM, STEM and STEM-EDX micrographs are acquired with a Talos F200X (S) TEM system (ThermoFisher, high-brightness X-FEG emitter) equipped with a Ceta 16 Megapixel CMOS camera.

Electrode sheet resistance. The electric sheet resistance of the electrodes was measured with a four-point probe (Ossila) on a 5 × 10 mm^2 sample (further details in S4).

Results and discussion

sPOSS characterization

IEC. sPOSS with an IEC of 2.78 mmol g^{-1} (determined by titration) has been synthesized by sulfonation of oPOSS (Fig. 1a). The relatively low IEC value suggests a sulfonation degree of ~45% or 3.7 sulfonic acid groups per sPOSS molecule (Fig. 1b). This is not in agreement with the published data by Hartmann-Thompson *et al.*[9] but in agreement with the observations of Fauzi *et al.*[22] who could not achieve full sulfonation by a similar synthesis route.

ATR-IR. Successful modification of oPOSS is confirmed by ATR-IR (Fig. 1c). Both the spectrum of oPOSS and sPOSS are similar to what was reported by Fauzi.[22] For oPOSS we observe a strong peak at 1085 cm^{-1} which is attributed to the Si–O–Si vibration. The peak at 1425 (Si–C) and the peaks between 680 and 770 cm^{-1} (Si–Ph) vibrations represent the phenyl rings on the silsequioxane cage.[22–24] The peaks at 3000–3100 cm^{-1} are attributed to aromatic C=C and C–H vibrations.[24] With sPOSS, peaks get broadened due to the introduction of the sulfonic acid group. Additionally, new peaks and shoulders appear due to the introduction of the sulfonic acid group. The shoulder at 1140 cm^{-1} and at 1150 cm^{-1} can be attributed to the introduced SO_3H group.[9] The peaks at 936 cm^{-1}, 804 cm^{-1} and 1650 cm^{-1} represent out-of-plane bending of aromatic rings indicating a meta-substitution of the phenyl ring.[22,24,25] Additionally, we see a broad OH peak introduced (3700 cm^{-1} −3000 cm^{-1}). This peak originates from absorbed water. The strong broadening of the peak indicates strong H-bonding.[24] With these findings we can conclude that sPOSS has been synthesized. Note that Fauzi *et al.* reported that the sulfonation of oPOSS with chlorosulfonic acid might lead to fractured cages. However, we don't observe any silanol (3750 cm^{-1}) vibrations indicating no significant loss of aromatic groups or broken cages.[22]

Protonic bulk conductivity. Protonic conductivity of the synthesized sPOSS bulk material shows conductivities similar to other state-of-the-art fluorine-free materials (see Fig. S2.1). It has a slightly lower conductivity than Nafion and sPPP[26] (of which Pemion® is a derivative), especially at low hydration numbers (λ) but has comparable conductivities to sPPS.[5]

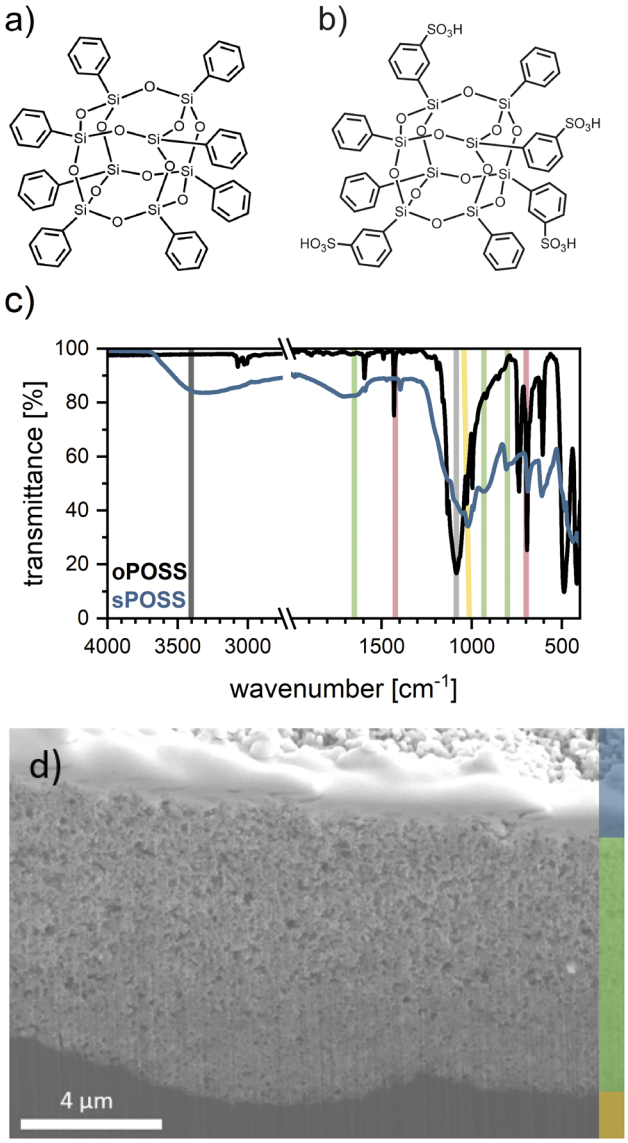

Fig. 1 (a) structure of oPOSS, (b) structure of sPOSS (sulfonation degree of 50%); (c) FT-IR of oPOSS (black) and sPOSS (blue)vertical lines indicate modes of interest: black: OH, gray: Si–O–Si, red: Si–Ph, green: meta substituted aromatic rings, yellow: SO_3 group; (d) SEM cross-section of cathode catalyst layer of sPOSS-0.2 imaged at an angle of 52°: blue: protective metallisation layer, green: catalyst layer, yellow: membrane.

Showing promising properties for the application as a protonic conductor in the catalyst layer.

Stability at operating conditions. To assess the hydrolytic stability of the synthesized sPOSS material, the sample was exposed to a water vapor atmosphere at 110 °C for six days (see Fig. S5a). At the beginning of the experiment the sample exhibited a sharp increase in mass due to water uptake (17 wt%). Once water absorption stabilized, the mass remained constant for the remainder of the experiment. This behavior suggests that sPOSS exhibits good stability under fuel cell operating conditions over extended periods. Additionally, the sPOSS was analyzed by ATR-IR after the hydrolytic stability test

(Fig. S5b). Here, no significant changes could be observed. The intensity of the water peak does not change, indicating no change in the adsorbed water, as well as there is no formation of a peak corresponding to silanol groups (3750 cm^{-1}), indicating stable Si–O–Si bonds.

The water uptake of 17 wt% equals to 3.4 water molecules per sulfonic acid group, indicating only moderate swelling, which benefits the dimensional stability of catalyst layers.

Cathode morphology. To evaluate the cathode structure when using sPOSS as functional binder material, cross-sections were analysed using scanning electron microscope (SEM) equipped with an EDX detector (see Fig. 1d and S6). The FIB cross-section (Fig. 1d) reveals that the cathode catalyst layer of sPOSS-0.2 has a thickness of approximately 9.8 ± 0.6 μm, which is in line with the ~10 μm reported in the literature for cathodes utilizing similar catalysts on carbon supports.[27]

EDX analysis (Fig. S6) of the material distribution at the micrometer scale did not reveal any clustering of specific elements, suggesting uniform mixing of the ink components and the absence of de-mixing during ink drying. This indicates the formation of a homogeneous catalyst layer.

Additionally, TEM micrographs were acquired (Fig. S7) by spay-coating the ink onto a TEM grid. The contrast between sPOSS and carbon was too low to resolve individual sPOSS molecules in TEM. In STEM-EDX (Fig. S7c and d), a clear Si signal was detected, indicating that at least some sPOSS molecules are attached to the carbon. Further analysis of the EDX elemental maps indicates a homogeneous distribution of sPOSS on the surface of the carbon particles, which can be derived from the apparent ringlike structure which appears due to the projection geometry where the electron beam passes through more material at the edges of the particles, resulting in higher contrast at the rims.

Optimising sPOSS content in the cathode catalyst layer

In this study, the sPOSS material was exclusively incorporated into the cathode catalyst layer, as the cathode typically presents more severe performance limitations in PEM fuel cells due to the sluggish oxygen reduction reaction (ORR) kinetics, higher proton transport demands, and thicker catalyst layers required for sufficient activity. In contrast, the anode was kept constant and fabricated using a commercial PEMion®-based ink formulation. This approach ensures that only the cathode ionomer was varied, allowing for a more controlled comparison of different cathode ink compositions, as the anode and membrane remained identical across all tests.

To find the best performing sPOSS to platinum on carbon (Vulcan® XC72) ratio (I/C) on the cathode, cells with different cathode I/C ratios; I/C = 0.1 (sPOSS-0.1), I/C = 0.2 (sPOSS-0.2), and I/C = 0.3 (sPOSS-0.3) are compared based on performance and protonic resistance at different RH as well as ECSA and mass activity.

ECSA. For all I/C ratios, similar ECSA values between 41 ± 4 and 45 ± 6 m^2 g^{-1} are measured, with variations attributed only to run-to-run variance (Fig. 2a). With an average measured ECSA of 43 m^2 g^{-1} the ECSA is approximately 30% higher than what was previously measured (33 m^2 g^{-1}), by Pescher *et al.*,[28] under the same conditions for PFSA-based electrodes. This difference may result from variations in ionomer–platinum interactions and swelling behavior. Yazili-Marini *et al.*[29] reported that the high swelling of PFSAs at high RH can lead to the passivation of active sites, which could explain why sPOSS provides more free reaction sites on platinum.

Catalyst mass activity. A similar trend is observed for the catalyst mass activity (Fig. 2a). All three cells show similar mass activities, around 59 A g^{-1}, except for sPOSS-0.1, which shows a slightly lower mass activity of 54 A g^{-1}. This reduction could be linked to a higher protonic resistance in the catalyst layer due to the lower ionomer binder content, reducing platinum utilization.[30] Overall the mass activity is 15–22% lower than what was measured previously for PFSA.[28] This reduction in mass-activity might be related to phenyl poisoning[31] or due to a difference in protonic conductivity.[30] Compared to sPPS, an ionomer that also suffers from both sulfone and phenyl poisoning, the loss in mass activity of sPOSS is less pronounced. For sPPS, a 75% lower mass activity compared to PFSA has been reported.[29]

Cathode protonic resistance. Protonic resistance evaluation shows a clear correlation between protonic resistance and sPOSS content (Fig. S8). At 80% RH, sPOSS-0.1 has the highest protonic resistance (4 Ω cm^2), followed by sPOSS-0.2 (1.3 Ω cm^2) while sPOSS-0.3 has approximately ten times lower protonic resistance (0.4 Ω cm^2).

This trend is exacerbated at a lower RH of 50% and leads to overall higher protonic resistances. For sPOSS-0.1 the resistance increases by a factor of 3.7, to 14.9 Ω cm^2, whereas for sPOSS-0.3 the resistance increases the least by a factor of 2.6 to 1.1 Ω cm^2. sPOSS-0.2 lies in-between with an increase of a factor of 3.0 to 3.5 Ω cm^2. This suggests that there are percolation issues that increase with low relative humidity, with sPOSS-0.3 being the least affected. Comparing protonic resistance to a Pemion®-based reference system we observe similar resistances in the catalyst layer. As high surface area carbon was used for the Pemion® reference its dependency on RH could be larger compared to the RH dependency of the sPOSS samples, which are using Vulcan type catalyst support.

Cell performance. As shown in Fig. 2c and d, sPOSS-0.2 (I/C = 0.2) achieves the best overall performance. The performance characteristics can be analysed based on two key trade-offs: (1) performance in the kinetic regime at low current densities and (2) performance in the ohmic and mass transport limited regime at higher current densities.

At high RH (95 °C, 80% RH, Fig. 2c) sPOSS-0.2 exhibits the highest performance across the entire polarization curve for the sPOSS-based cells. Both sPOSS-0.1 and sPOSS-0.3 show lower performance at low current densities than sPOSS-0.2. However, sPOSS-0.1 gains performance towards higher current densities, achieving similar limiting currents as sPOSS-0.2. The low performance of sPOSS-0.3 in the kinetic area is not fully understood as all previous characterizations such as ECSA and protonic resistance suggested performance on par or better than sPOSS-0.2.

One indication is given when analysing the electrical sheet resistance of the catalyst layers (Fig. S4.1). Here, an increase in resistance is observed with higher sPOSS content, which may

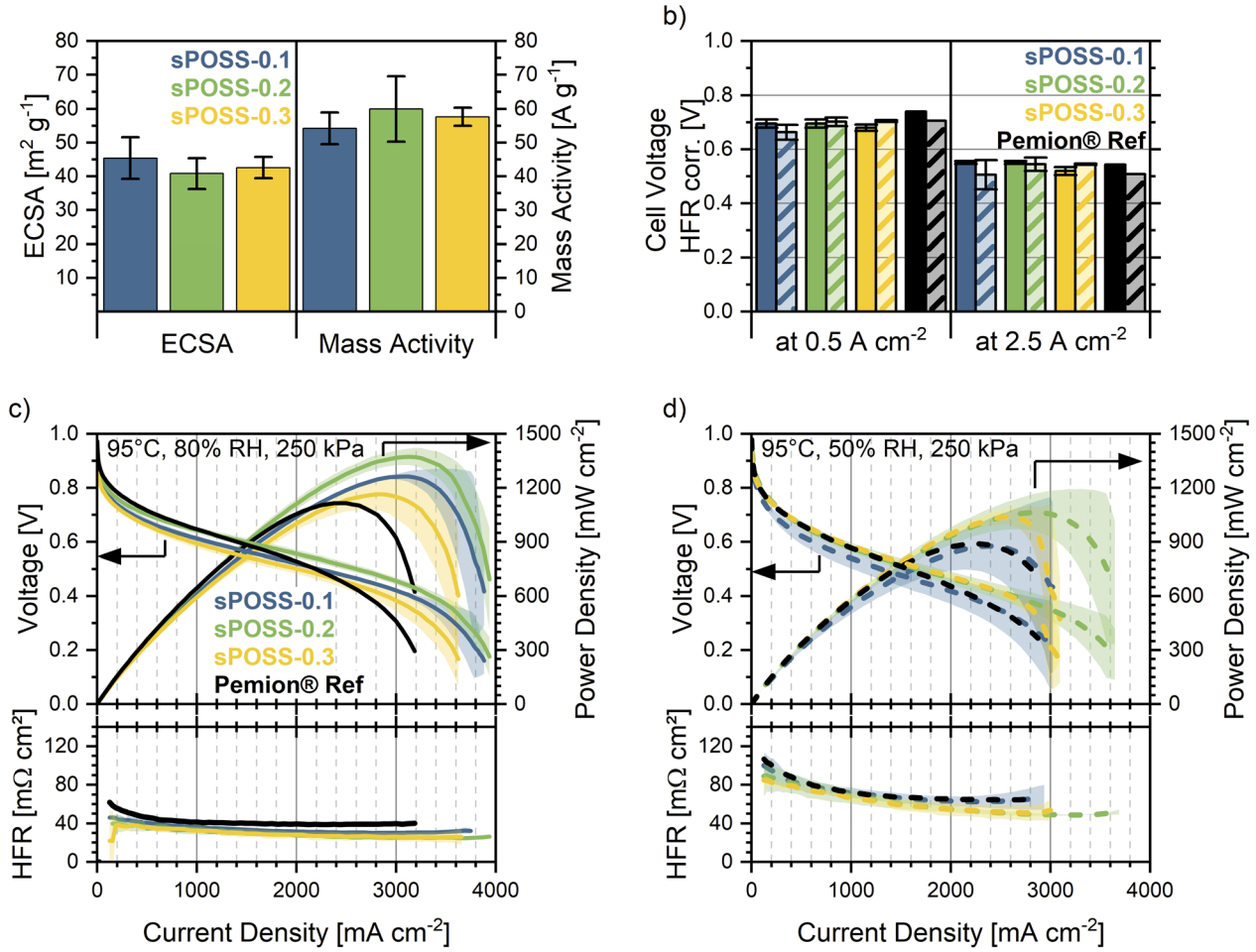

Fig. 2 *In situ* characterisation and performance data: sPOSS-0.1 (blue), sPOSS-0.2 (green) and sPOSS-0.3 (yellow). As reference, a state-of-the-art Pemion® cell is plotted in black. (a) ECSA data (left panel) and mass activity data (right panel); (b) HFR-free-voltage at 0.5 and 2.5 A cm^{-2} calculated from the polarization curves above (Fig. 2c and d). Solid bars are measured at 80% RH and dashed bars at 50%RH. (c) Polarization curve with power density and HFR in air at 95 °C, 80% RH, 250 kPa back-pressure: UI polarization curves(left axis), power density (right axis); (d) Polarization curve with power density and HFR in air at 95 °C, 80% RH, 250 kPa back-pressure: UI polarization curves (left axis), power density (right axis).

cause an inhomogeneous current distribution and impact cell performance.

Under dryer operating conditions (95 °C, 50% RH, Fig. 2d), sPOSS-0.3 performs similarly to sPOSS-0.2 except at high current density. This aligns with previous observations of protonic resistance and performance at high RH. As the protonic resistance changes the least for sPOSS-0.3, performance is less affected with respect to the other sPOSS cells at reduced RH. Only in the mass transport region, it is limited, probably due to high ionomer content reducing the porosity of the electrodes, hindering gas transport. sPOSS-0.1 on the other hand significantly loses performance at low current densities making it the least suitable for dry operation. This behaviour correlates with the observed sharp increase in protonic resistance under dry conditions, leading to performance loss across the entire current range.

Comparing sPOSS-0.2 to a state-of-the-art Pemion® reference[6,30] at 80% RH, it is observed that in the low current density regime, Pemion® performs better compared to sPOSS-0.2 (717 mV *vs.* 702 mV at 500 mA cm^{-2}). However, with increasing current density the sPOSS cells achieve higher performance with respect to the Pemion®-based cell (*i.e.*, sPOSS-0.2 surpasses Pemion® over about 1.2 A cm^{-2}). This supports the initial idea of using a particle-based system as an electrode ion conductor as the gas mass transport should be increased due to the additional porosity. Pemion®'s better performance at low current densities is probably due to its superior proton conductivity at low λ. Additionally, it suggests that the initial theory of less catalyst ionomer interaction due to steric hindrance decreasing phenyl poisoning is not true, as both systems show very similar losses in the kinetic regime.

Switching to dry conditions, all curves converge but at current densities above 1500 mA cm^{-2} sPOSS-based cells surpasses the Pemion®-based cell.

Power density. sPOSS-0.2 demonstrates a 20% higher maximum power density compared to Pemion® in both wet and

dry conditions (Fig. 2c and d). Meanwhile, sPOSS-0.3 matches the maximum power density of the Pemion® reference at 80% RH. However, under dryer conditions, sPOSS-0.3 exhibits a 17% increase in maximum power density compared to Pemion®, aligning it with sPOSS-0.2.

HFR compensated cell performance. To get a better insight into the electrode performance at different RH, HFR-free potentials at 500 mA cm^{-2} and 2500 mA cm^{-2} are compared Fig. 2b). Interestingly, the performance at 80% and 50% RH is nearly the same for sPOSS-0.2 and sPOSS-0.3, indicating that electrode performance is independent of RH within this range. Interestingly the performance of sPOSS-0.3 increases, even though slightly, at dryer conditions (705 mV *vs.* 680 mV at 500 mA cm^{-2} under 50% RH *vs.* 80% RH). This behavior is unexpected. One possible explanation might be better water management at low RH for sPOSS and/or that the decrease in electrode performance, caused by reduced proton conductivity, is offset by the increased oxygen partial pressure resulting from the lower water content in the gas stream. Only sPOSS-0.1 shows the expected trends of decreasing electrode performance with decreasing RH. This observation is supported by the relatively small decrease in protonic conductivity for sPOSS-0.2 and especially for sPOSS-0.3. Notably, sPOSS-0.3 maintains the same protonic conductivity at 50% RH as sPOSS-0.2 does at 80% RH (see Fig. S8), indicating that the protonic losses in the electrode are relatively minor even under drier conditions. This limited loss in proton conductivity, combined with potentially improved oxygen transport due to lower water content and thus higher effective oxygen concentration, may contribute to the stable electrode performance across a broad RH range. The influence of oxygen concentration on electrode performance is further illustrated in Fig. S9. Here, current hold measurements were conducted at 0.5 and 2.0 A cm^{-2} under 50% and 80% RH in air, as well as at 50% RH with 18% O_2 in N_2, the latter providing a comparable oxygen partial pressure to air at 80% RH. The HFR-free cell voltages at 50% RH with 18% O_2 are similar to, or slightly lower than, those at 80% RH in air. In contrast, the HFR-free voltages under dry conditions in air are again slightly higher than those measured at 80% RH, further suggesting that reduced water content and increased oxygen availability can offset limitations in proton transport and help maintain electrode performance.

O_2 limiting current. As sPOSS-based cells exhibit higher performance in the mass transport-limited regime than Pemion®-based cells, pressure-independent mass transport is evaluated, as it mainly reflects gas transport losses occurring in the catalyst layers (see Fig. S10).[32] It is observed that the pressure-independent mass transport for sPOSS-0.2 and sPOSS-0.3 is 15 s cm^{-2}, which is 30% lower than the value, 21 s cm^{-2}, measured for Pemion®. This supports the initial hypothesis of improved mass transport behavior using sPOSS particles compared to ionic polymers. This is likely due to higher porosity and lower local transport resistance, as the particle-based system cannot fully encase the catalyst particles.

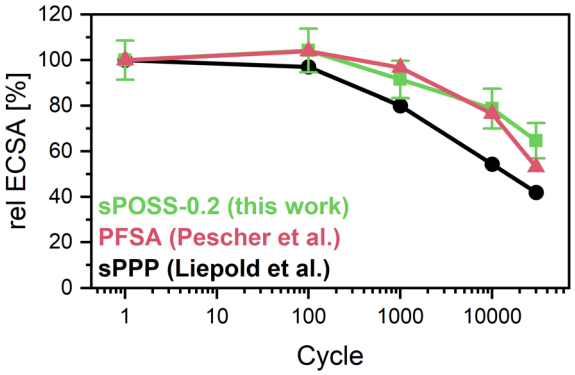

Fig. 3 Long-term stability of sPOSS cells: relative loss in ECSA in relation to the potential cycles (square-wave 0.5 V-0.95 V); cell with electrode sPOSS-0.2 (green), PFSA literature (red)[28] and sPPP literature (black)[20]

Voltage cycling. Long-term stability tests were conducted using a platinum dissolution test with 30k cycles as it operates under high relative humidities and elevated potentials.[21] As these conditions might attack the sPOSS-based catalyst layer. Additionally, it is shown in literature that different ionomer materials can have an influence on cell degradation behavior under these conditions.[20,28]

Looking at the ECSA retention (Fig. 3), we observe losses very comparable to Pescher *et al.* who utilized the same catalyst in a fully PFSA-based cell.[28] Comparing BOT and EOT performance (Fig. S11) we observe a severe drop in performance (*i.e.*, 70 mV at 1 A cm^{-2}, but no failure). This loss is slightly higher compared to Pescher *et al.*,[28] as they observed a loss of about 60 mV at 1 A cm^{-2}. When comparing to sPPP degradation data, published by Liepold *et al.*,[20] ECSA retention of sPOSS is higher, as sPPP has a stronger initial drop in ECSA during voltage cycling. This shows that sPOSS-based catalyst layers have a similar stability as PFSA-based catalyst layers.

Conclusions and outlook

We synthesized and tested a novel polyhedral oligomeric silsesquioxane-based proton-conducting material (sPOSS) for use in the fuel cell cathode catalyst layer. Initial studies demonstrate promising performance, already comparable to that of commercial materials, highlighting its potential as an innovative material in this field. Furthermore, preliminary stability tests under prolonged exposure to high relative humidity and potential cycling reveal encouraging trends.

We observed that the particle-based system boosts high-current density performance while the protonic resistance is still sufficient to enable good performance.

The application of sPOSS in fuel cell electrodes is of interest due to the low costs and high availability. Additionally, sPOSS electrode inks should be easy to formulate, as only the dissolution of sPOSS is important. In contrast, for polyelectrolytes, the solvent system must be carefully adjusted to ensure not only dissolution but also the correct polymer conformation. This

difference might enable dry-casting as only sufficient mixing is necessary. Dry-casting would enable higher production rates at lower prices.[33]

However, to establish sPOSS as a widely used electrode material, further research is essential. A key area of focus should be optimizing the sPOSS synthesis to selectively obtain intact cage or fractured cage to investigate their inherent properties as well as finding the balance between proton conductivity and solubility/stability by varying the ion exchange capacity (IEC). Additionally, a deeper understanding of long-term stability under diverse operating conditions, as well as the degradation mechanisms under prolonged stress, must be explored. Furthermore, future research should investigate whether the observed benefits of sPOSS arise solely from its morphology as an assumed hard-sphere particle, or whether its open, cage-like molecular structure also contributes to the improved cell performance. Of interest would be if sPOSS could be used in conjunction with other hydrocarbon materials, both benefiting from the unique properties of each other.

Author contributions

J. Stiegeler: conceptualization, methodology, investigation, data curation, writing – original draft, writing – review & editing, visualization, project administration. S. K. Killian: methodology, investigation, writing – original draft, writing – review & editing, visualization. M. Viviani: investigation, methodology, resources, writing – review & editing. H. Liepold: resources, formal analysis, writing – review & editing. C. Klose: funding acquisition, project administration, supervision, writing – review & editing. A. Münchinger: conceptualization, supervision, writing – review & editing. T. de Wild: conceptualization, supervision, writing – review & editing.

Conflicts of interest

There are no conflicts of interest to declare.

Data availability

Data for this article, including ATR-IR, cell performance, and durability as well as oxygen-transport resistance data is available. See DOI: **https://doi.org/10.60493/ha9ex-ds217**

Supplementary information (SI): data supporting this article. See DOI: **https://doi.org/10.1039/d5ta02947c**.

Acknowledgements

The authors acknowledge funding from the Federal Ministry of Education and Research of Germany (BMBF) through the project FC-RAT (Grant 03EW0011B) and the project FC-CAT (Grant 03SF0579B). We acknowledge the Freiburg Center for Interactive Materials and Bioinspired Technologies (FIT) for providing access to the FIB-SEM and TEM. We want to thank Klaus-Dieter Kreuer (Max Planck Institute and Hahn-Schickard) for carrying out bulk proton conductivity measurements. We thank Frederik Brendel (Electrochemical Energy Systems, IMTEK – Department of Microsystems Engineering, University of Freiburg) and Edgar Cruz-Ortiz (Hahn-Schickard) for measuring FIB-SEM cross sections and SEM-EDX. We also want to thank Dr Ralf Thomann (Freiburg Center for Interactive Materials and Bioinspired Technologies (FIT)) for measuring TEM and STEM-EDX. During the preparation of this work, the authors utilized ChatGPT to enhance text clarity and readability. All generated content was subsequently reviewed and edited as necessary, and the authors assume full responsibility for the final publication.

References

1 P. Casal, B. González-Gaya, Y. Zhang, A. J. F. Reardon, J. W. Martin, B. Jiménez and J. Dachs, Accumulation of Perfluoroalkylated Substances in Oceanic Plankton, *Environ. Sci. Technol.*, 2017, **51**, 2766–2775, DOI: **10.1021/acs.est.6b05821**.

2 W. Wang, G. Rhodes, J. Ge, X. Yu and H. Li, Uptake and accumulation of per- and polyfluoroalkyl substances in plants, *Chemosphere*, 2020, **261**, 127584, DOI: **10.1016/j.chemosphere.2020.127584**.

3 M. Feng, R. Qu, Z. Wei, L. Wang, P. Sun and Z. Wang, Characterization of the thermolysis products of Nafion membrane: A potential source of perfluorinated compounds in the environment, *Sci. Rep.*, 2015, **5**, 9859, DOI: **10.1038/srep09859**.

4 ECHA, The PFAS Restriction Proposal, **https://echa.europa.eu/documents/10162/2082415/2023-02-07_pfas+media+briefing_en.pdf**, accessed 10 April 2025.

5 M. Schuster, K.-D. Kreuer, H. T. Andersen and J. Maier, Sulfonated Poly(phenylene sulfone) Polymers as Hydrolytically and Thermooxidatively Stable Proton Conducting Ionomers, *Macromolecules*, 2007, **40**, 598–607, DOI: **10.1021/ma062324z**.

6 H. Nguyen, F. Lombeck, C. Schwarz, P. A. Heizmann, M. Adamski, H.-F. Lee, B. Britton, S. Holdcroft, S. Vierrath and M. Breitwieser, Hydrocarbon-based Pemion™ proton exchange membrane fuel cells with state-of-the-art performance, *Sustain. Energy Fuels*, 2021, **5**, 3687–3699, DOI: **10.1039/D1SE00556A**.

7 H. Liepold, H. Nguyen, P. A. Heizmann, C. Klose, S. Vierrath and A. Münchinger, Gas Transport Resistance of Hydrocarbon-Based Catalyst Layers in Proton-Exchange Membrane Fuel Cells, *J. Electrochem. Soc.*, 2024, **171**, 54509, DOI: **10.1149/1945-7111/ad44db**.

8 M. Adamski, N. Peressin and S. Holdcroft, On the evolution of sulfonated polyphenylenes as proton exchange membranes for fuel cells, *Mater. Adv.*, 2021, **2**, 4966–5005, DOI: **10.1039/D1MA00511A**.

9 C. Hartmann-Thompson, A. Merrington, P. I. Carver, D. L. Keeley, J. L. Rousseau, D. Hucul, K. J. Bruza, L. S. Thomas, S. E. Keinath, R. M. Nowak, D. M. Katona and P. R. Santurri, Proton-conducting polyhedral oligosilsesquioxane nanoadditives for sulfonated polyphenylsulfone hydrogen fuel cell proton exchange

membranes, *J. Appl. Polym. Sci.*, 2008, **110**, 958–974, DOI: 10.1002/app.28665.

10 N. A. M. Nor, J. Jaafar and J.-D. Kim, Improved properties of sulfonated octaphenyl polyhedral silsequioxane cross-link with highly sulfonated polyphenylsulfone as proton exchange membrane, *J. Solid State Electrochem.*, 2020, **24**, 1185–1195, DOI: 10.1007/s10008-020-04594-2.

11 M. Y. Ansari, K. B. Ansari, Inamuddin and S. J. A. Rizvi, Silica and Sulfonated Silica Functionalized Nexar Nanocomposite Membranes for Application in Proton Exchange Membrane Fuel Cell, *Arab. J. Sci. Eng.*, 2023, **48**, 16187–16199, DOI: 10.1007/s13369-023-08085-0.

12 J. B. A. Joseph Helen Therese, R. Gayathri, K. Selvakumar, M. Ramesh Prabhu and P. Sivakumar, Incorporation of sulfonated silica nano particles into polymer blend membrane for PEM fuel cell applications, *Mater. Res. Express*, 2019, **6**, 115336, DOI: 10.1088/2053-1591/ab4a3b.

13 R. Alipour Moghadam Esfahani, H. M. Fruehwald, F. Afsahi and E. B. Easton, Enhancing fuel cell catalyst layer stability using a dual-function sulfonated silica-based ionomer, *Appl. Catal., B*, 2018, **232**, 314–321, DOI: 10.1016/j.apcatb.2018.03.080.

14 R. Angayarkanni, A. Ganesan, M. Dhelipan, S. Karthikeyan, N. Mani and P. Thiyagarajan, Self-humidified operation of a PEM fuel cell using a novel silica composite coating method, *Int. J. Hydrogen Energy*, 2022, **47**, 4827–4837, DOI: 10.1016/j.ijhydene.2021.11.103.

15 M. R. Berber, M. Imran, H. Nishino and H. Uchida, Suppression of Membrane Degradation Accompanied with Increased Output Performance in Fuel Cells by Use of Silica-Containing Anode Catalyst Layers, *ACS Appl. Mater. Interfaces*, 2023, **15**, 13219–13227, DOI: 10.1021/acsami.3c01392.

16 A. Olejnik, B. Sztorch, D. Brząkalski and R. E. Przekop, Silsesquioxanes in the Cosmetics Industry-Applications and Perspectives, *Materials*, 2022, **15**(3), DOI: 10.3390/ma15031126.

17 K. C. Neyerlin, W. Gu, J. Jorne and H. A. Gasteiger, Determination of Catalyst Unique Parameters for the Oxygen Reduction Reaction in a PEMFC, *J. Electrochem. Soc.*, 2006, **153**, A1955, DOI: 10.1149/1.2266294.

18 H. Schulenburg, J. Durst, E. Müller, A. Wokaun and G. G. Scherer, Real surface area measurements of Pt3Co/C catalysts, *J. Electroanal. Chem.*, 2010, **642**, 52–60, DOI: 10.1016/j.jelechem.2010.02.005.

19 S. Kabir, D. J. Myers, N. Kariuki, J. Park, G. Wang, A. Baker, N. Macauley, R. Mukundan, K. L. More and K. C. Neyerlin, Elucidating the Dynamic Nature of Fuel Cell Electrodes as a Function of Conditioning: An ex Situ Material Characterization and in Situ Electrochemical Diagnostic Study, *ACS Appl. Mater. Interfaces*, 2019, **11**, 45016–45030, DOI: 10.1021/acsami.9b11365.

20 H. Liepold, H. Sannemüller, P. A. Heizmann, J. Stiegeler, T. de Wild, C. Klose, R. Alink, S. Vierrath, S. Holdcroft and A. Münchinger, Back to black: utilizing unsupported Pt for thin cathodes in PFSA-free PEM fuel cells, *Sustainable Energy Fuels*, 2025, DOI: 10.1039/D5SE00809C.

21 U.S. DRIVE Partnership Plan, Roadmaps, and Accomplishments, Fuel Cell Technical Team Roadmap, 2017, https://www.energy.gov/eere/vehicles/articles/us-drive-fuel-cell-technical-team-roadmap, accessed 10 April 2025.

22 F. B. Fauzi and J.-D. Kim, Comprehensive studies on sulfonated octaphenyl polyhedral silsesquioxane (SPOSS) using sulfuric acid: Structural analysis and composite crosslinked SPPSU/SPOSS membranes, *J. Membr. Sci.*, 2024, **702**, 122756, DOI: 10.1016/j.memsci.2024.122756.

23 P. Launer and B. Arkles, in *Silicon Compounds : Silanes and Silicones*, ed. B. Arkles and G. L. Larson, Gelest Inc., Morrisville, PA, 3rd edn, 2013, pp. 175–178.

24 V. Söderholm, J. Esteban and D. Vogt, Synthesis of a H-Sulfo-POSS catalyst and application in the acetalization of glycerol with 2-butanone to yield a biofuel additive, *Catal. Sci. Technol.*, 2021, **11**, 4529–4538, DOI: 10.1039/D1CY00344E.

25 S. Subianto, M. K. Mistry, N. R. Choudhury, N. K. Dutta and R. Knott, Composite polymer electrolyte containing ionic liquid and functionalized polyhedral oligomeric silsesquioxanes for anhydrous PEM applications, *ACS Appl. Mater. Interfaces*, 2009, **1**, 1173–1182, DOI: 10.1021/am900020w.

26 M. Adamski, T. J. Skalski, E. M. Schibli, M. Killer, Y. Wu, N. Peressin, B. J. Frisken and S. Holdcroft, Molecular branching as a simple approach to improving polymer electrolyte membranes, *J. Membr. Sci.*, 2020, **595**, 117539, DOI: 10.1016/j.memsci.2019.117539.

27 G. S. Harzer, J. N. Schwämmlein, A. M. Damjanović, S. Ghosh and H. A. Gasteiger, Cathode Loading Impact on Voltage Cycling Induced PEMFC Degradation: A Voltage Loss Analysis, *J. Electrochem. Soc.*, 2018, **165**, F3118–F3131, DOI: 10.1149/2.0161806jes.

28 F. Pescher, J. Stiegeler, P. A. Heizmann, C. Klose, S. Vierrath and M. Breitwieser, Pt/C catalysts synthesized in a commercial particle atomic layer deposition system enabling improved durability in fuel cells, *RSC Adv.*, 2024, **14**, 32358–32369, DOI: 10.1039/d4ra04708g.

29 D. Yazili-Marini, L. T. Fogang, E. Marini, T. Morawietz, G. Titvinidze, J. Bansmann, M. Hölzle and L. Jörissen, Exploring the integration of sulfonated poly(phenylene sulfone) ionomers into the cathode catalyst layers of proton exchange membrane fuel cells, *J. Power Sources*, 2025, **641**, 236896, DOI: 10.1016/j.jpowsour.2025.236896.

30 H. Liepold, A. Bird, P. A. Heizmann, H. Fadlullah, H. Nguyen, C. Klose, S. Holdcroft, A. Kusoglu, S. Vierrath and A. Münchinger, High protonic resistance of hydrocarbon-based cathodes in PEM fuel cells under low humidity conditions: Origin, implication, and mitigation, *J. Power Sources*, 2024, **624**, 235537, DOI: 10.1016/j.jpowsour.2024.235537.

31 Y. Choi, M. Z. Win, W. Oo, J. Min, K. Ko, Y. Kim, H. Choi, S. S. Chougule, D. Khikmatulla, K. B. Yi and N. Jung, Experimental simulation study on the poisoning effect of hydrocarbon-based ionomers on Pt catalysts for fuel cells,

Electrochem. Commun., 2023, **157**, 107602, DOI: **10.1016/j.elecom.2023.107602**.

32 N. Nonoyama, S. Okazaki, A. Z. Weber, Y. Ikogi and T. Yoshida, Analysis of Oxygen-Transport Diffusion Resistance in Proton-Exchange-Membrane Fuel Cells, *J. Electrochem. Soc.*, 2011, **158**, B416, DOI: **10.1149/1.3546038**.

33 M. D. Bouguern, A. K. Madikere Raghunatha Reddy, X. Li, S. Deng, H. Laryea and K. Zaghib, Engineering Dry Electrode Manufacturing for Sustainable Lithium-Ion Batteries, *Batteries*, 2024, **10**, 39, DOI: **10.3390/batteries10010039**.